Title
First in vivo traumatic brain injury imaging via magnetic particle imaging

Journal
Physics in Medicine and Biology, 62(9)

ISSN
0031-9155

Authors
Orendorff, R
Peck, AJ
Zheng, B
et al.

Publication Date
2017-04-05

DOI
10.1088/1361-6560/aa52ad

Peer reviewed

IOP Publishing | Institute of Physics and Engineering in Medicine Physics in Medicine & Biology

Phys. Med. Biol. **62** (2017) 3501–3509 https://doi.org/10.1088/1361-6560/aa52ad

First *in vivo* traumatic brain injury imaging via magnetic particle imaging

Ryan Orendorff[1], Austin J Peck[2], Bo Zheng[1], Shawn N Shirazi[2], R Matthew Ferguson[3], Amit P Khandhar[3], Scott J Kemp[3], Patrick Goodwill[4], Kannan M Krishnan[3,5], George A Brooks[2], Daniela Kaufer[2] and Steven Conolly[1,6]

[1] Department of Bioengineering, University of California, Berkeley, CA, United States of America
[2] Department of Integrative Biology, University of California, Berkeley, CA, United States of America
[3] LodeSpin Labs LLC, Seattle Washington, United States of America
[4] Magnetic Insight Inc, Alameda CA, United States of America
[5] Department of Materials Science and Engineering, University of Washington, WA, United States of America
[6] Depertmant of Electrical Engineering and Computer Science, University of California, Berkeley, CA, United States of America

E-mail: sconolly@berkeley.edu

Received 10 October 2016, revised 21 November 2016
Accepted for publication 8 December 2016
Published 5 April 2017

Abstract

Emergency room visits due to traumatic brain injury (TBI) is common, but classifying the severity of the injury remains an open challenge. Some subjective methods such as the Glasgow Coma Scale attempt to classify traumatic brain injuries, as well as some imaging based modalities such as computed tomography and magnetic resonance imaging. However, to date it is still difficult to detect and monitor mild to moderate injuries. In this report, we demonstrate that the magnetic particle imaging (MPI) modality can be applied to imaging TBI events with excellent contrast. MPI can monitor injected iron nanoparticles over long time scales without signal loss, allowing researchers and clinicians to monitor the change in blood pools as the wound heals.

Keywords: traumatic brain injury, magnetic particle imaging, iron nanoparticles, tracer imaging

(Some figures may appear in colour only in the online journal)

1. Introduction

The centers for disease control and prevention estimates 1.6–2.1 million emergency visits for traumatic brain injury (TBI) annually in the US alone, with additional cases unaccounted for or untreated (Langlois *et al* 2004, 2006). Despite the prevalence of TBI in humans and various animal models of TBI (Albert-Weissenberger and Sirén 2010), classifying the severity of injury remains an open challenge.

In clinical settings, diagnoses and recovery are assessed using neuropsychological batteries and the glasgow coma scale (GCTS), with efforts to develop a more robust classi□cation system under way (Teasdale and Jennett 1974, Saatman *et al* 2008). Depending on initial clinical presentation, physicians may order x-ray computed tomography (CT) or diffusion tensor magnetic resonance imaging (DTI) to visualize potential hemorrhages, lesions, or contusions caused by severe impacts (Liu *et al* 1999, Lee and Newberg 2005). While these techniques are suitable for severe TBI injuries, many mild to medium grade impacts go undiagnosed, untreated, or are deemed too mild to necessitate imaging (Lee and Newberg 2005). Severity is determined by observing motor, re□ex, cognitive, and histological changes using the modi□ed neurological severity score (MNSS), cognitive tasks, and post mortem analysis, respectively (Saatman *et al* 2006, Flierl *et al* 2009).

Magnetic particle imaging (MPI) is a promising new modality that images a distribution of superparamagnetic iron oxide (SPIO) nanoparticles inside the body (Gleich and Weizenecker 2005). mpi has many advantageous properties, including a safe tracer (Reimer and Balzer 2003), zero ionizing radiation, minuscule changes in magnetic reporter signal over time, 200 nM sensitivity (Zheng *et al* 2015, 2016), fast image acquisition and reconstruction (Konkle *et al* 2013a, 2013b), robust linearity and shift invariance (LSI) properties (Lu *et al* 2013), and sub-millimeter resolution (Yu *et al* 2016). In addition, particles can be tracked for long periods of time in both the blood (with a half-life of approximately 3 hours) and inside cells (with a half-life on the order of months (Keselman *et al* 2016)). Due to their size, the iron oxide tracers are excreted through the liver and spleen, instead of the kidneys (Keselman *et al* 2016). This has prompted interest in using one SPIO agent (Ferumoxytol) as a kidney-safe magnetic resonance imaging (MRI) T_1 MRI contrast agent for patients with chronic kidney disease (Lu *et al* 2010), who are at risk for contrast induced nephropathy from iodine contrast agents (Stacul *et al* 2011).

Compared to contrast-enhanced CT and MRI, MPI has favourable contrast since there is no signal from background tissue; MPI produces images with excellent contrast to noise ratio (CNR) as only the iron particles produce a signal. This property makes MPI well suited for angiography and blood pool imaging, as only the blood appears in the resulting image due to the particles staying inside the vasculature. The only limitation to imaging capillary-level perfusion or blood volume is signal to noise ratio (SNR). Typically, in CT angiography (CTA) and MR angiography (MRA), our ability to discern a 5% blood volume in voxels with capillaries (without larger-diameter blood vessels) is obscured by so-called 'partial volume' effects; essentially the background signal variations are indistinguishable from the minute variations of contrast agent in the capillaries. Since MPI does not detect the tissue surrounding a capillary—only the particles in the capillaries themselves—it is mostly robust to this partial volume effect.

In this report, we present preliminary data and methods showing that MPI can provide high contrast to noise ratio (CNR) images of internal bleeding, and in particular cerebral bleeding caused by TBI. This application requires all the fundamental advantages of MPI, including excellent contrast, sensitivity, spatial resolution and long circulation time.

2. Basics of MPI

The formation of images with MPI are described in detail here: (Gleich and Weizenecker 2005, Goodwill and Conolly 2010, 2011, Konkle *et al* 2013a, Lu *et al* 2013, Saritas *et al* 2013, Ferguson *et al* 2015). We brie□y summarize the basic theory behind MPI.

SPIOs are nanoscale iron particles with a diameter of approximately 30 nm or less that have a single magnetic domain that, in aggregate, align to an applied magnetic □eld almost instantaneously and without any coercivity. The magnetic □eld of a population of particles in response to an applied magnetic □eld can be modeled by the Langevin function (Goodwill and Conolly 2010), as shown in □gure 1. For small amplitude applied magnetic □elds, the particle population creates a net magnetization with an approximately linear dependence on the applied □eld. However, at larger applied □eld strengths, the particles 'saturate', meaning that nearly all of the particles have aligned with the applied □eld and therefore higher □eld strengths have diminishing effects on the resulting magnetization response from the particles.

Magnetic particle imaging exploits this saturation phenomenon to image only a small number of particles within a volume. Magnets in MPI are designed to oppose each other and create a magnetic □eld gradient, with a FFR in the center that experiences zero applied □eld (to within some tolerance). This arrangement allows particles to linearly respond to an applied magnetic □eld inside the FFR while eliminating signal outside of the FFR due to the saturation of the particles. To produce an image, the FFR is rastered over space to acquire the magnetization response of the particles as the FFR passes over them. As MPI detection is done through inductive means, the derivative of the magnetization response is captured. As described in Goodwill and Conolly (2010) and Lu *et al* (2013), MPI is a LSI system with a spatially-invariant 1D point-spread function (PSF)—the derivative of the Langevin function—as shown in □gure 1.

2.1. Nanoparticle design

Designing SPIO particles suitable for MPI is a rich and active area of research (Ferguson *et al* 2015, Kemp *et al* 2016). SPIO particles are ideally monodisperse, and each iron core is surrounded by an organic coating. The physics of the iron core and the chemistry of the coating allows for tailoring the particles to many applications, allowing researchers to alter attributes including blood circulation times, particle clearance routes, ability to permeate tissues, adsorption, cellular uptake, and ability to act as a biomarker. As an extra degree of freedom, polydisperse particle distributions have been shown to produce MPI signals.

The design of iron core has implications for the imaging physics as well; in particular, image resolution and signal intensity per gram of iron can be improved by choosing the appropriate iron crystal formulation. Some other properties must be carefully tuned to the application at hand. A particle with a signi□cant blood half-life may be unsuitable for imaging transient phenomenon such as blood volume or □ow changes, while a particle with a short half-life may not experience signi□cant uptake in some biological models. Tailoring the blood half-life is quite important if multiple imaging sessions of a dynamic phenomenon are to be performed serially; if the particles are too slow to clear before a new injection is given then particles from prior scans may introduce an undesirable baseline signal and disrupt attempts to analyze the dynamic of interest.

In this manuscript, we used LS-13 nanoparticles from LodeSpin Labs. These particles have excellent signal per gram of iron and superb image resolution. Of importance to TBI is that the circulation half-life of LS-13 is approximately four to six hours due to the hydrophilic coating

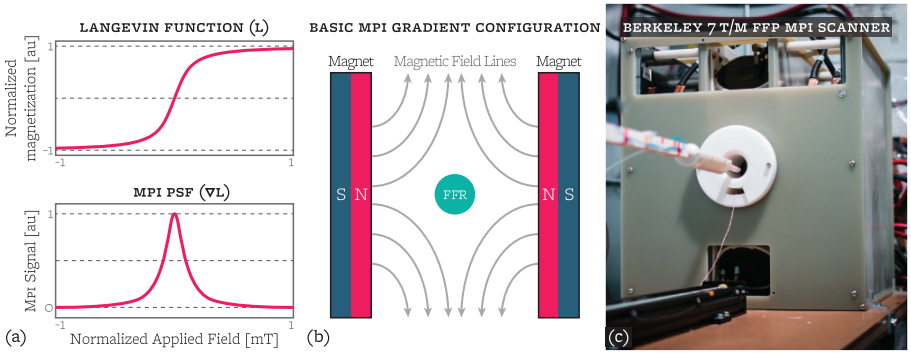

Figure 1. Introduction on magnetic particle imaging (MPI). (a top) MPI abides by the physics of the SPIO nanoparticles that it images. The SPIO particles have a nonlinear magnetization response to an applied field, characterized by the Langevin function. When the applied magnetic field is low, the particles have an approximately linear response to the applied field; however, when the applied magnetic field is strengthened, the response magnetization in the SPIO particles saturates. (a bottom) MPI detects the derivative of the SPIO magnetic response, which forms MPI's PSF. (b) All MPI scanners must make a gradient magnetic field to exploit the Langevin physics. In this case, two permanent magnets are placed opposite each other to create a magnetic field gradient. In the middle of the magnets is a field free region (FFR) where the particles have a near linear dependence on the applied field: any particles not located in the FFR experience a saturating applied field, and therefore produce no signal. The MPI scanner creates an image by rastering the FFR over space to acquire signal from the SPIO particle distribution at each sample point. (c) An image of the Berkeley FFP scanner used in this report.

surrounding the iron particle core (see figure 3), which potentially allows particles to infiltrate interstitial spaces over time. These particles clear from the blood stream to the liver.

3. Materials and methods

To assess the ability of MPI to detect internal hemorrhaging, a closed head TBI model was used with two Fisher-344 female rats. We briefly describe the associated induction procedure; see figure 2 for a graphical representation of the technique.

3.1. Closed skull TBI induction

All TBI animal experiments were approved by the UC Berkeley Animal Care and Use Committee (ACUC).

Both animals were female Fisher-344 rats. The TBI impact animal weighted 207 g while the control weighed 136 g.

Each rat was anesthetized using 3% isoflurane and a bolus of 2.4 mg kg^{-1} LS-13 SPIOs was administered via tail vein injection. One animal was then placed in a rectangular animal bed filled with a plush bedding material underneath a custom designed closed impact TBI device (figure 2). The animal's head was placed under a bolt with a hex nut attached to the threaded end, with the hex nut gently resting on the animal's skull near the lambda skull suture. A 454 g weight—consisting of a Falcon tube filled with lead shot pellets—was then calibrated to drop from one meter above the top of the bolt. A forepaw pinch was performed to confirm that the

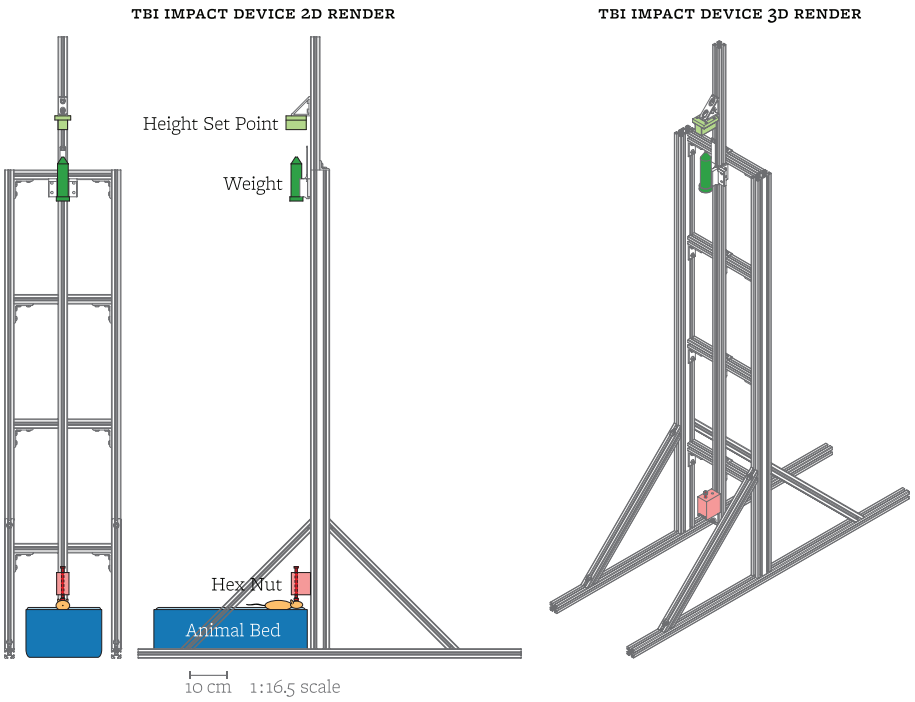

Figure 2. Diagram of the TBI impact device, which imparts a closed skull TBI injury onto an animal. An impact procedure is brie□y described as follows. A 50 ml Falcon tube (dark green) is □lled with lead pellets to the desired weight and the height set point block (light green) is set to the desired drop height. The animal (light orange) is placed in the animal bed (dark blue) on top of a soft bedding material (light blue). The weight is then dropped onto a bolt resting on the animal's skull (dark red). The bolt is held in place by a 3D printed part (light red). Impact device is drawn to a 1:16.5 scale with respect to the page.

animal was still under the effects of the iso□urane, after which the weight was released. The second animal went through the same procedure as a sham control without the weight drop.

After being in the TBI impact device, both animals were allowed to wake up to check for signs of lethal trauma such as erratic movements, high frequency whisker twitches, and (in the worst case) mortality.

3.2. MPI imaging protocol

A detailed design of the Berkeley □eld free point (FFP) scanner can be found in the literature (Saritas *et al* 2013); here we describe only the imaging parameters.

Following the injury and post-operative checks, both animals were imaged in the Berkeley FFP MPI scanner with gradient strengths of 7 T m^{-1} by 3.5 T m^{-1} by 3.5 T m^{-1} in x, y, and z, respectively. The drive □eld amplitude was set to 40 mTpp at a frequency of 20.225 kHz along the axis of the bore (z). Selection □eld electromagnets moved the FFP in the x and y directions to acquire samples on a rectilinear grid for one XY slab through the imaging volume. The width of each slab was 0.91 cm in z. 40 XY slabs were acquired at increments of 0.2 cm in z.

Scans were performed with the following parameters: 4.0 cm by 3.75 cm by 8.5 cm field of view (FOV) (x,y,z) using LS-13 SPIO particles. The acquisition time was measured to be approximately ten minutes.

X-space image reconstruction—including DC recovery and slab stitching—was performed as described by Lu *et al* (2013). No deconvolution was applied to the image.

The longitudinal analysis was performed by imaging the animals over successive days using the same scan parameters. Before each scan, the animals were anesthetized with isoflurane and kept under anesthesia for the duration of the scan. The images were then registered with the initial image using a cross-correlation method (Guizar-Sicairos *et al* 2008). Regions of interest were then selected within these images and the maximum signal in each region over time was plotted; see figure 3.

Anatomical x-ray images were taken using a Kubtec XPERT 40 cabinet, with an energy range of 10–50 kV, a tube current up to 1.0 mA, and a resolution of 10 lp mm^{-1}. The animals were placed in contact-mode into the cabinet and imaged using the auto-calibration setting.

4. Results

Signal in the region affected by the TBI impact can be clearly seen in the MPI scans, both immediately after and a few days following the impact (see figure 3). The acquired MPI images indicate that SPIO particles accumulated quickly after impact at some location around the skull and persisted for a two week period. Additionally, x-ray scans of the TBI animal indicated a small skull fracture in a $\in$-shape near lambda in the XZ x-ray projection.

The clearance rate of particles at the impact site and locations within certain regions of the head were significantly retarded from the estimated six hour blood half-life of LS-13 particles (figure 3). The half-life of the particle signal in the impact region was approximately four days for the TBI animal, while no signal above the noise was detected in the equivalent area of the sham animal.

In both animals, signal accumulated in small regions on both sides in the neck. Due to the location of the signal and the clearance pathway, these regions are suspected to be lymph nodes. In both animals, the lymph nodes started to appear in the MPI images after approximately half a day. The clearance half-life rate for the control animal was three days, while the TBI animal experienced a slightly delayed clearance of four days. The lymph node signal was still visible in the TBI animal at the last time point of eleven days, while the lymph signal in the control animal was still visible at the last time point of nine days. The bottom right pane of figure 3 provides a more detailed illustration of the particle signal over time in both the impact region and lymph region.

5. Discussion

The acquired MPI images indicate that the bleeding was significant enough to allow for SPIO particles to infiltrate into blood pools in the interstitial space. Signal decay of the control is consistent with typical clearance of SPIO through the circulatory system and liver (Jain *et al* 2008, Longmire *et al* 2008). Furthermore, appearance of signal lateral to the cervical spine with unique decay rates suggests SPIO clearance mechanisms from cerebral interstitium are facilitated through the brain's lymphatic system which have been shown to drain to submandibular and cervical lymph nodes (Bradbury *et al* 1981, Mathieu *et al* 2013). Recent reports have also shown meningeal localization of these vessels (Aspelund *et al* 2015, Louveau *et al* 2015). While further experiments must be performed for validation, the clearance through lymphatic nodes provides a method by which to observe and analyze the lymphatic pathways in the skull.

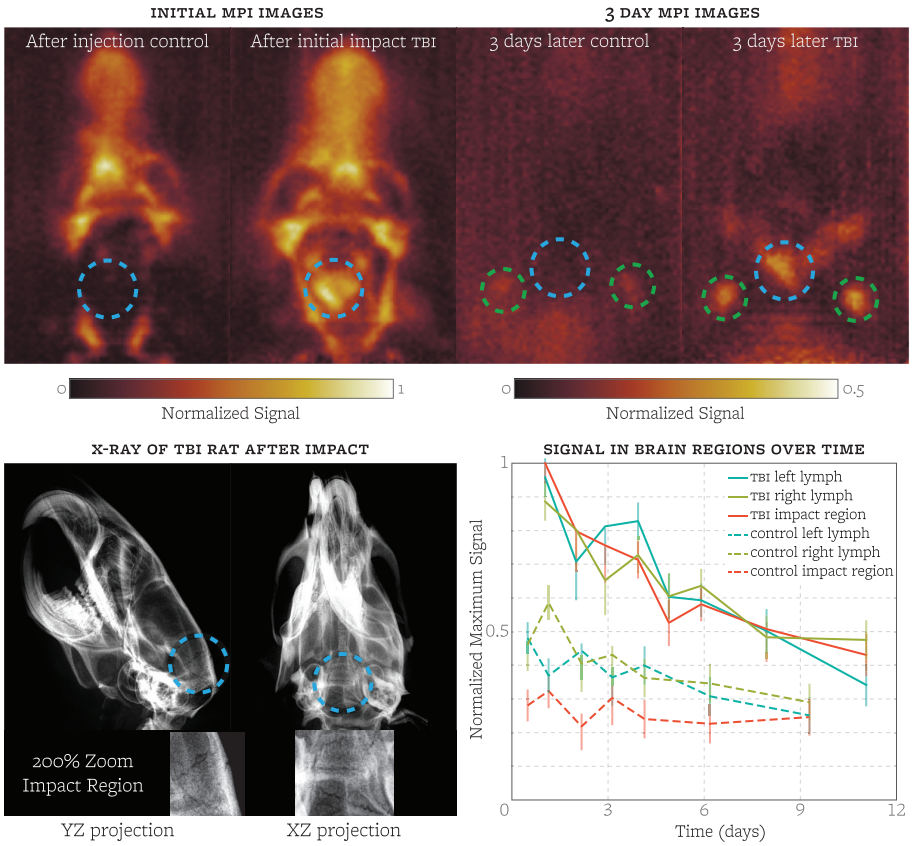

Figure 3. (Top left) XZ maximum intensity projection (MIP) of both animals after injection/impact. Note the large hemorrhage in the TBI animal. (Top right) MIP of the animals after 3d; blue circle represents the impact site, green circles indicate lymph nodes. The TBI rat continues to have signi□cant signal from the hemorrhage and inside the lymph nodes, unlike the control. The □eld of view was 4.00 cm by 3.75 cm by 8.5 cm (x,y,z). (Bottom left) X-ray images taken of the rat that underwent the TBI impact. A faint ∈-shaped fracture can be seen at the back of the head in the XZ projection. (Bottom right) Signal from the SPIO nanoparticles over time inside the skull. The clearance rate at the point of injury and the lymph nodes in the TBI rat is signi□cantly slower than in the control animal. Error bars represent two standard deviations of the background noise at each time point.

The results show potential for MPI in clinical settings. The bleeding caused by the TBI was visible both immediately after the injury as well as many days into the future. The ability to monitor the change in the impact zone provides a metric for measuring the healing process as blood is cleared from the interstitial space.

In this study particles were injected prior to injury: this scenario is unlikely to occur in clinical practice. As such, further studies should be performed to determine the uptake of particles after an injury occurred. Of particular interest would be the uptake over time, as it would indicate whether the particles would need to be injected soon after the injury was suspected or if this injection could be delayed until arriving at a clinic.

The ability to image hemorrhages in MPI makes it a potential augmentation or replacement for imaging hemorrhages using CT. While CT is able to image severe hemorrhages quite well without a contrast agent, it remains an open challenge to image mild to medium severity injuries (Lee and Newberg 2005). Part of the challenge lies in the contrast to noise ratio in imaging modalities like CT, where signal of interest must be compared to a similarly strong signal from background tissues. MPI does not detect background tissues, allowing the hemorrhage to show up well against a signi□cantly dimmer background.

6. Conclusion

Our work represents the □rst visualization of primary brain injury and associated hematoma in any TBI model using MPI. Currently investigators and clinicians rely on changes in the neurological severity score (NSS) and GCTS, which primarily evaluate cognition, motor function, and loss of re□exes to evaluate injury severity. We demonstrate that MPI can be used to determine site, severity, and depth of bleeding from a closed skull TBI model regardless of brain regions targeted and behavioral manifestation of injury.

Furthermore, by demonstrating the ability to detect extravasation of blood associated SPIO into extravascular space we propose that MPI is a modality well suited to localizing and quantifying internal bleeding regardless of pathophysiological cause. Additional experiments will be performed to determine if the SPIO particles in□ltrate the blood brain barrier (BBB) after a TBI event, which would enable a quantitative measurement of BBB leakiness both spatially and temporally. These results demonstrate a potential future for noninvasive diagnosis of internal bleeding for patients suffering from trauma in the emergency setting using MPI.

Acknowledgments

We are grateful for funding support from the Keck Foundation Grant 009323, NIH 1R01EB019458, NIH 1R24MH106053, and a UC Discovery Grant. LodeSpin Labs is also grateful for NIH 2R42EB013520-02A1. Ryan Orendorff would like to thank the NSF GRFP for funding support.

References

Albert-Weissenberger C and Sirén A L 2010 Experimental traumatic brain injury *Exp. Trans. Stroke Med.* **2** 1

Aspelund A, Antila S, Proulx S T, Karlsen T V, Karaman S, Detmar M, Wiig H and Alitalo K 2015 A dural lymphatic vascular system that drains brain interstitial □uid and macromolecules *J. Exp. Med.* **212** 991–9

Bradbury M, Cserr H and Westrop R 1981 Drainage of cerebral interstitial □uid into deep cervical lymph of the rabbit *Am. J. Physiol.-Renal Physiol.* **240** F329–36

Ferguson R M *et al* 2015 Magnetic particle imaging with tailored iron oxide nanoparticle tracers *IEEE Trans. Med. Imaging* **34** 1077–84

Flierl M A, Stahel P F, Beauchamp K M, Morgan S J, Smith W R and Shohami E 2009 Mouse closed head injury model induced by a weight-drop device *Nat. Protocols* **4** 1328–37

Gleich B and Weizenecker J 2005 Tomographic imaging using the nonlinear response of magnetic particles *Nature* **435** 1214–7

Goodwill P W and Conolly S M 2010 The x-space formulation of the magnetic particle imaging process: 1-D signal, resolution, bandwidth, SNR, SAR, and magnetostimulation *IEEE Trans. Med. Imaging* **29** 1851–9

Goodwill P W and Conolly S M 2011 Multidimensional x-space magnetic particle imaging *IEEE Trans. Med. Imaging* **30** 1581–90

Guizar-Sicairos M, Thurman S T and Fienup J R 2008 Ef□cient subpixel image registration algorithms *Opt. Lett.* **33** 156–8
Jain T K, Reddy M K, Morales M A, Leslie-Pelecky D L and Labhasetwar V 2008 Biodistribution, clearance, and biocompatibility of iron oxide magnetic nanoparticles in rats *Mol. Pharmaceutics* **5** 316–27
Kemp S J, Ferguson R M, Khandhar A P and Krishnan K M 2016 Monodisperse magnetite nanoparticles with nearly ideal saturation magnetization *RSC Adv.* **6** 77452–64
Keselman P, Yu E, Zhou X, Goodwill P, Ferguson R M, Kemp S, Khandhar A, Krishnan K, Zheng B and Conolly S 2016 Magnetic particle imaging as a tool for tracking *in vivo* biodistribution and long-term tracking of iron oxide nanoparticle tracers and therapeutics *World Molecular Imaging Congress*
Konkle J J, Goodwill P W, Carrasco-Zevallos O M and Conolly S M 2013a Projection reconstruction magnetic particle imaging *IEEE Trans. Med. Imaging* **32** 338–47
Konkle J J, Goodwill P W, Saritas E U, Zheng B, Lu K and Conolly S M 2013b Twenty-fold acceleration of 3D projection reconstruction MPI *Biomed. Technik/Biomed. Eng.* **58** 565–76
Langlois J A, Rutland-Brown W and Thomas K E 2004 *Traumatic Brain Injury in the United States: Emergency Department Visits, Hospitalizations, and Deaths* (Atlanta, GA: Department of Health and Human Services, Centers for Disease Control and Prevention, Division of Acute Care, Rehabilitation Research and Disability Prevention, National Center for Injury Prevention and Control)
Langlois J A, Rutland-Brown W and Wald M M 2006 The epidemiology and impact of traumatic brain injury: a brief overview *J. Head Trauma Rehabil.* **21** 375–8
Lee B and Newberg A 2005 Neuroimaging in traumatic brain imaging *NeuroRx* **2** 372–83
Liu A Y, Maldjian J A, Bagley L J, Sinson G P and Grossman R I 1999 Traumatic brain injury: diffusion-weighted MR imaging □ndings *Am. J. Neuroradiol.* **20** 1636–41(PMID: 10543633)
Longmire M, Choyke P L and Kobayashi H 2008 Clearance properties of nano-sized particles and molecules as imaging agents: considerations and caveats *Future Med.* **3** 703–17
Louveau A *et al* 2015 Structural and functional features of central nervous system lymphatic vessels *Nature* **523** 337–41
Lu K, Goodwill P W, Saritas E U, Zheng B and Conolly S M 2013 Linearity and shift invariance for quantitative magnetic particle imaging *IEEE Trans. Med. Imaging* **32** 1565–75
Lu M, Cohen M H, Rieves D and Pazdur R 2010 FDA report: ferumoxytol for intravenous iron therapy in adult patients with chronic kidney disease *Am. J. Hematol.* **85** 315–9
Mathieu E, Gupta N, Macdonald R L, Ai J and Yücel Y H 2013 *In vivo* imaging of lymphatic drainage of cerebrospinal □uid in mouse *Fluids Barriers CNS* **10** 1
Reimer P and Balzer T 2003 Ferucarbotran (resovist): a new clinically approved RES-speci□c contrast agent for contrast-enhanced MRI of the liver: properties, clinical development, and applications *Eur. Radiol.* **13** 1266–76
Saatman K E, Duhaime A C, Bullock R, Maas A I, Valadka A and Manley G T 2008 Classi□cation of traumatic brain injury for targeted therapies *J. Neurotrauma* **25** 719–38
Saatman K E, Feeko K J, Pape R L and Raghupathi R 2006 Differential behavioral and histopathological responses to graded cortical impact injury in mice *J. Neurotrauma* **23** 1241–53
Saritas E U, Goodwill P W, Croft L R, Konkle J J, Lu K, Zheng B and Conolly S M 2013 Magnetic particle imaging (MPI) for NMR and MRI researchers *J. Magn. Reson.* **229** 116–26
Stacul F *et al* 2011 Contrast induced nephropathy: updated ESUR contrast media safety committee guidelines *Eur. Radiol.* **21** 2527–41
Teasdale G and Jennett B 1974 Assessment of coma and impaired consciousness: a practical scale *Lancet* **304** 81–4
Yu E, Bishop M, Zheng B, Ferguson R M, Khandhar A, Kemp S, Krishnan K, Goodwill P and Conolly S 2016 First demonstration of *in vivo* cancer magnetic particle imaging with iv-administered passive long-circulating spios *World Molecular Imaging Congress*
Zheng B, Marc P, Yu E, Gunel B, Lu K, Vazin T, Schaffer D V, Goodwill P W and Conolly S M 2016 Quantitative magnetic particle imaging monitors the transplantation, biodistribution, and clearance of stem cells *in vivo Theranostics* **6** 291
Zheng B, Vazin T, Goodwill P W, Conway A, Verma A, Saritas E U, Schaffer D and Conolly S M 2015 Magnetic particle imaging tracks the long-term fate of *in vivo* neural cell implants with high image contrast *Sci. Rep.* **5** 14055